Contrib Mineral Petrol (1986) 92:413–427

Contributions to Mineralogy and Petrology

Cooling and uplift patterns in the Lepontine Alps South Central Switzerland and an age of vertical movement on the Insubric fault line

Anthony J. Hurford
Laboratory for Isotope Geology, University of Berne, Erlachstraße 9a, CH-3012 Berne, Switzerland

Abstract. 96 new fission track (FT) apatite and zircon, K/Ar and Rb/Sr biotite and muscovite ages are presented for 19 samples (mainly acid gneisses) from a 40 km traverse through the Lepontine Alps in the Maggia Valley, South Central Switzerland. Plotting measured mineral ages against assumed system closure temperatures yields cooling rates for each sample. The entire profile shows a fairly uniform Late Neogene-Recent mean uplift rate of ~0.5 mm/a, confirmed by a gradient of FT apatite age with elevation. Cooling from higher temperatures occurred earlier in the south, where uplift rates of ~2.2 mm/a in the Steep Belt (root zone) indicate >9 km Early Miocene uplift of the northern Pennine block. This uplift started before 23 Ma and is interpreted as resulting from a major phase of backthrusting along the Insubric Line, and as dating the formation of the mylonite belt. Estimated cooling rates constrain the timing of Lepontine Mid-Tertiary metamorphism: 3 schematic models are proposed which also consider published Rb/Sr, K/Ar mica and hornblende and U/Pb monazite ages. Slow cooling, differential initial heating and subsequent cooling of different parts of the Central Alps and post-38 Ma cooling with syntectonic metamorphism at ~27 Ma are postulated as alternative interpretations of isotopic data and geologic evidence. From extrapolation between K/Ar and Rb/Sr mica ages and apatite FT ages, 240 ± 50° C is proposed as the closure temperature for the retention of fission tracks in zircon.

Introduction and background

The complex history of the Alps, including their origins, formation, polyphase deformation, polyphase metamorphism and uplift, centres on the interaction of the Eurasian and African tectonic plates and the intervening Tethyan geosyncline. Various synoptic accounts of the Alpine story have been proffered, see for example Dewey and Bird 1970; Milnes 1978; Rybach et al. 1980; Trümpy 1980.

In summary, Early- to Mid Jurassic opening of the Central Atlantic initiated sinistral movement of Africa relative to Eurasia and the consequent development of the passive margin Piemont-Ligurin ocean (Bernoulli and Lemoine 1980) at roughly the present-day site of the Appenines and Alps. Extensive sedimentation during the Jurassic and Early Cretaceous was accompanied by typical ophiolite volcanics. Mid Cretaceous opening of the Southern Atlantic produced an anti-clockwise rotation of the African plate with consequent compression of Tethys and the continental margins. Initial Eoapline compression is poorly understood: crustal shortening in Tethys produced new islands and ridges, furnishing detritus for large scale flysch deposition. High pressure Eoalpine metamorphism, dated as Cretaceous (Dal Piaz et al. 1972), may have resulted from the northern margin of Tethys being the site of an island arc-continent collision (Dewey and Bird 1970) with lithospheric subduction (Hunziker 1974).

Mesoalpine shortening and closure of the Tethyan geosyncline resulted from the northward movement of the Apulian plate, either driven by Africa or fused to it. Whether tectonism was continuous or a series of discrete phases or multiple collisions is unclear. Major Mesoalpine deformation occurred between the Upper Cretaceous and Eocene-Oligocene with formation of the Pennine nappes from Central Tethyan Mesozoic sediments and Pre-Triassic crystalline basement. Continent-continent collision resulted in overthrusting of Austroalpine nappes from the southern Tethyan shelf and northern Apulian continental margin. In the deeply buried Pennine nappes temperatures rose sufficiently to produce amphibolite facies metamorphism. The Insubric Line (Gansser 1968) sharply divides the Lepontine Alps, with Alpine structures and metamorphism in the north from the Prealpine structures and metamorphism of the Southern Alps. Modern reasoning places the continent-continent suture further north, represented today by the Zermatt ophiolites in W. Switzerland and the Lower Austroalpine-Pennine boundary in E. Switzerland. From Oligocene times, appreciable uplift of the Alpine pile only occurred north of the Insubric Line, with erosion of the Pennine and Austroalpine nappes to give molasse deposits to the north and south. Uplift was accompanied by minor syn-to postkinematic granite emplacement. Neoalpine phases of thrusting of sediments in the northern Tethyan margin produced the Helvetic nappes which overrode the Hercynian Aar massif (e.g., Milnes and Pfiffner 1977). Development of the so-called root zone or Steep Belt at the southern border of the Pennine zone represents an even later stage of compressive deformation (Milnes 1974) presumably by a northward push of the Apulian plate. The southern margin of the Lepontine Alps is marked by a steeply dipping mylonite zone up to 1 km thick, resulting from movement along the Insubric Line.

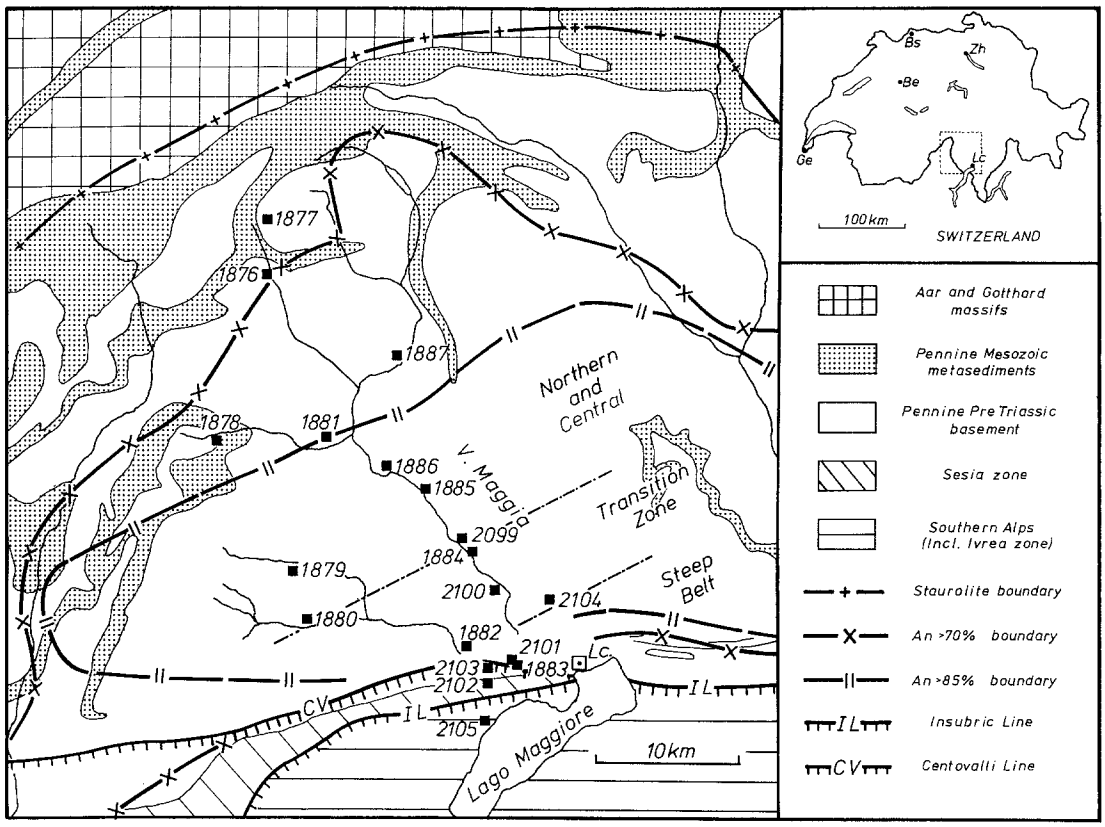

Fig. 1. Sample location map. Base map is taken from Wagner et al. (1977) and the metamorphic isograds from Jäger et al. (1967). Isograds are omitted in the vicinity of Locarno for clarity. *Lc* Locarno; *Be* Berne; *Bs* Basle; *Zh* Zürich; *Ge* Geneva

The Lepontine Alps expose, within the broad uplifted region of the Aar-Ticino Culmination, the deepest levels of the Pennine zone, with polyphase deformation and metamorphism of Alpine age (Ayrton and Ramsay 1974; Milnes 1974). The Barrovian-type metamorphic mineral assemblages have received detailed description (see Bearth 1958; Wenk and Keller 1969; Niggli 1970; Frey et al. 1980 and references therein) and reveal roughly concentric isograd surfaces cross-cutting nappe boundaries. The peak of prograde Mesoalpine metamorphism is considered by Hunziker (1969) and Jäger (1973) to have occurred 38–35 Ma ago – the Lepontine Phase – based upon Rb/Sr phengite ages from the outer Lepontine area which are interpreted as formation ages: accordingly, all mineral ages in the higher grade central and southern Lepontine are regarded as cooling ages subsequent to this metamorphic climax. In an alternative hypothesis (Köppel and Grünenfelder 1975, 1978) concordant monazite U/Pb ages are considered as recording the time of mineral formation under high grade metamorphic conditions ~27 Ma in the Southern Steep Belt adjacent to the Insubric Line, 20–24 Ma further north in the tectonically deeper, more slowly cooling Lepontine. Jäger (1979) interprets such monazite results as cooling ages.

Metamorphism appears to have been mainly synchronous with post-nappe recumbent folding, high-temperature producing ductility in the basement rocks, giving the present-day sheetlike form seen in many Pennine nappes (Milnes 1974). Post-kinematic development of idiomorphic kyanite, staurolite and garnet porphyroblasts (Ayrton and Ramsay 1974) indicate the persistence of amphibolite facies conditions beyond deformation.

Sampling

The present work reports a systematic study of samples along a traverse through the Lepontine Alps using the fission track (FT), K/Ar and Rb/Sr dating methods. 19 samples, each of about 30 kg, were collected along a 40 km traverse through the Maggia Valley of Canton Ticino, South Central Switzerland (Fig. 1). The section lies 5–10 km west of the Swiss Geotraverse running from Basle to Chiasso (Rybach et al. 1980). Exact sample localities and brief descriptions of the samples are given in Appendix 1. Most samples are acid basement gneisses, with a metamorphosed dyke from Arcegno (KAW 2102) and a pegmatite from Ponte Brolla (KAW 1883). Most samples lie within the Pennine Zone: in the north at Lago Bianco the Pennine nappe front is approached with Mesoalpine staurolite grade metamorphism, whilst to the southeast sub-horizontally foliated gneisses show increasing anorthite content of plagioclase co-existing with calcite. At the southern end of the traverse, samples lie in the Southern Steep Belt with vertically or sub-vertically foliated gneisses. This steep zone is bounded to the south by the approximately east-west trending Insubric fault system: samples KAW 2102 and 2103 come from between two fault lines: the Insubric mylonite belt to the south and a later zone of cataclasis to the north – the Centovalli Fault. A single sample, KAW 2105, comes from the Ivrea zone, south of the Insubric Line at Porto Ronco.

Widely differing temperatures for the retention of daughter isotopes and fission tracks in different minerals, permit detailed modelling of the thermal histories of samples along the profile (after Wagner et al. 1977), the calculation of uplift rates, and offer time constraints for the last major period of vertical movement on the Insubric Fault Line.

Experimental procedures

From each 30 kg sample, high purity concentrates of apatite, zircon, biotite and, where present, muscovite were separated using

Table 1. Synopsis of Rb/Sr, K/Ar and FT dating results on Maggia samples. (Note: all ages are given in Ma., with 1 σ errors)

Sample and locality	Altitude (meters)	Rb/Sr muscovite	K/Ar muscovite	Rb/Sr biotite	K/Ar biotite	FT zircon	FT apatite	FT apatite (recalculated to 350 m altitude)
Northern and Central Maggia:								
KAW 1877 Lago Bianco	2090	22.5±1.9	16.8±0.2	15.4±0.2	15.4±0.2	13.5±0.7	7.8±0.8	3.5±0.4
KAW 1876 Val Bavona	1060	19.3±0.3	16.6±0.3	13.2±0.2	14.2±0.2	10.9±0.5	5.1±0.5	3.3±0.3
KAW 1887 Menzonio	630	17.6±2.1	17.2±0.2	15.7±0.2	15.9±0.2	13.2±1.5	7.6±0.7	6.9±0.6
KAW 1878 Bosco Gurin	1550	18.3±0.3	16.1±0.2	14.7±0.2	15.4±0.2	12.2±0.8	5.2±0.6	2.2±0.3
KAW 1881 Linescio	680	–	–	15.3±0.3	14.7±0.2	14.2±1.8	8.6±1.1	7.8±1.0
KAW 1886 Riveo	420	–	–	16.3±0.3	15.2±0.2	13.0±0.9	8.4±1.3	8.2±1.2
KAW 1885 Giumaglio Someo	360	–	18.5±0.2	16.2±0.3	16.3±0.2	13.3±0.7	9.1±0.7	9.1±0.7
KAW 1879 Valle Vergeletto	980	–	–	18.5±0.3	17.6±0.2	15.6±1.0	7.9±0.7	6.3±0.5
KAW 2099 Maggia	350	–	–	23.0±0.3	17.9±0.2	13.0±0.7	7.9±0.8	7.9±0.8
KAW 1880 Valle Onsernone	960	–	–	19.3±0.3	18.8±0.2	16.1±0.8	8.9±1.1	7.4±1.0
Transition Zone:								
KAW 1884 Moghegno	300	19.6±0.6	18.5±0.2	18.1±0.3	17.3±0.2	14.3±0.7	6.7±0.6	6.8±0.6
KAW 2100 Ronchi	630	26.0±0.9	19.5±0.2	18.7±0.2	19.3±0.2	16.8±0.9	8.0±0.7	7.3±0.6
KAW 2104 Cima della Trosa	1869	–	–	20.2±0.3	20.4±0.3	18.0±0.9	12.8±1.4	9.0±1.0
KAW 1882 Intragna	340	–	–	19.4±0.3	18.6±0.2	14.9±1.2	9.5±0.7	9.5±0.7
Southern Steep Belt:								
KAW 2101 Ponte Brolla	250	24.0±0.5	20.8±0.2	19.3±0.2	20.4±0.2	18.9±0.9	9.3±0.7	9.5±0.7
KAW 1883 Ponte Brolla (Pegmatite)	220	22.4±0.2	19.3±0.3	19.4±0.2	19.0±0.2	–	–	–
KAW 2103 Golino	250	22.9±1.0	20.5±0.2	19.2±0.2	19.4±0.2	18.8±1.2	10.1±0.8	10.3±0.9
KAW 2102 Arcegno	480	–	–	8.6±0.1	21.3±0.2	18.9±1.5	12.4±1.7	11.8±1.6
Ivrea Zone:								
KAW 2105 Porto Ronco	225	205 ±4	166 ±2	160 ±2	180 ±2	48.2±3.7	15.2±2.1	15.0±2.2

conventional crushing, Wilfley-table, shaking-table, magnetic and heavy-liquid techniques. In addition, a whole-rock fraction was prepared for each sample by grinding 100 g aliquots in an agate mill under pure ethanol for 15 h.

Fission track dating. Most apatites were analysed using the Population Method (Gleadow 1981) whereby spontaneous and induced tracks are revealed and counted in separate sample aliquots. Spontaneous tracks in the induced aliquot were annealed prior to irradiation by heating at 500° C for 5 h. After irradiation spontaneous and induced fractions were similarly mounted on glass in epoxy, polished to reveal internal surfaces and simultaneously etched in 1N HNO_3 at 20° C for 45 s. Because of the small number of crystals recovered, apatite from sample KAW 2105 was dated by the External Detector Method (EDM – see below). For each sample, track densities were determined on prismatic faces using a Leitz Orthoplan microscope at a nominal magnification of 1575 with a dry objective. Lengths of confined spontaneous tracks were measured with a Zeiss Morphomat 30 image analysis system. Confined tracks do not outcrop at the polished etched surface but intersect other etched tracks, cleavages or fractures, which facilitate the passage of etchant to the confined track (see Lal et al. 1968; Gleadow

Table 2. Fission track analytical data for Maggia samples and Fish Canyon age standards. (Note: zircon ages calculated with $\zeta_{612}=337.5\pm5$, $\zeta_{CN-1}=112.8\pm2.6$ and $\zeta_{CN-2}=120.6\pm3.6$; apatite ages calculated with $\zeta_{612}=323\pm19$, $\zeta_{CN-1}=108.6\pm6.5$ and $\zeta_{CN-2}=116.4\pm7.0$)

Sample and locality	Mineral	Irradiation no.	No. crystals	Spontaneous		Induced		$\overline{\varrho_s/\varrho_i}$	T_{612} (Ma)	T_{CN-1} (Ma)	T_{CN-2} (Ma)	Mean age (Ma) ($\pm1\sigma$)
				N_s	ϱ_s ($\times10^5$ t cm^{-2})	N_i	ϱ_i ($\times10^5$ t cm^{-2})					
KAW 1877	apatite	Bern-10	–	104	0.403	1133	10.6	–	7.8	7.7	8.0	7.8±0.8
Lago Bianco	zircon	Bern-4	15	1051	28.6	1654	45.0	–	13.3	13.9	13.4	13.5±0.7
KAW 1876	apatite	Bern-10	–	196	0.550	2398	22.43	–	5.1	4.9	5.2	5.1±0.5
Val Bavona	zircon	Bern-4	15	990	25.1	1928	48.9	–	10.7	11.2	10.8	10.9±0.5
KAW 1887	apatite	Bern-14	–	215	0.362	2850	9.60	–	7.6	7.5	7.5	7.6±0.7
Menzonio	zircon	Bern-9	8	865	31.1	1512	54.3	0.575	13.2	13.5	13.0	13.2±1.5
KAW 1878	apatite	Bern-10	–	87	0.247	1717	9.73	–	5.2	5.1	5.3	5.2±0.6
Bosco Gurin	zircon	Bern-9	5	433	31.7	821	60.1	–	12.2	12.4	11.9	12.2±0.8
KAW 1881	apatite	Bern-10	–	81	0.133	605	3.18	–	8.6	8.4	8.8	8.6±1.1
Linescio	zircon	Bern-7	10	560	26.7	1014	48.4	0.593	14.5	13.8	14.4	14.2±1.8
KAW 1886	apatite	Bern-10	–	56	0.157	690	3.87	–	8.4	8.2	8.6	8.4±1.3
Riveo	zircon	Bern-6	10	432	21.0	796	38.7	–	12.3	13.3	13.4	13.0±0.7
KAW 1885	apatite	Bern-10	–	298	1.67	4039	37.8	–	9.1	8.9	9.3	9.1±0.7
Giumaglio	zircon	FTD-113	9	883	56.7	1249	80.2	–	14.3	12.9	12.8	13.3±0.7
KAW 1879	apatite	Bern-10	–	302	0.353	1981	9.26	–	7.9	7.6	8.0	7.9±0.7
Valle Vergeletto	zircon	Bern-7	15	1085	34.7	1782	57.0	0.609	15.8	15.1	15.8	15.6±1.0
KAW 2099	apatite	Bern-14	–	130	0.365	995	9.31	–	7.9	7.8	7.8	7.9±0.8
Maggia	zircon	Bern-17	12	690	23.3	1243	42.0	–	13.1	12.9	12.9	13.0±0.7
KAW 1880	apatite	Bern-10	–	78	0.146	1005	3.38	–	8.9	8.7	9.1	8.9±1.1
Valle Onsernone	zircon	Bern-4	12	915	30.2	1206	39.9	–	15.9	16.6	16.0	16.1±0.8
KAW 1884	apatite	Bern-10	–	220	0.617	2032	19.0	–	6.7	6.6	6.9	6.7±0.6
Moghegno	zircon	FTD-113	12	993	35.8	1310	47.3	–	15.3	13.9	13.7	14.3±0.7
KAW 2100	apatite	Bern-14	–	295	0.828	2226	20.8	–	8.0	7.9	8.0	8.0±0.7
Ronchi	zircon	Bern-18	12	868	42.5	1249	61.1	–	17.1	16.3	17.0	16.8±0.9
KAW 2104	apatite	Bern-14	–	132	0.370	1033	5.80	–	12.9	12.8	12.8	12.8±1.4
Cima della Trosa	zircon	Bern-17	12	922	40.1	1197	52.1	–	18.1	17.9	17.9	18.0±0.9
KAW 1882	apatite	Bern-10	–	395	0.623	4020	13.5	–	9.5	9.3	9.7	9.5±0.7
Intragna	zircon	FTD-113	10	833	39.5	1133	53.8	0.750	15.1	13.7	13.6	14.1±1.2
KAW 2101	apatite	Bern-14	–	411	1.73	3986	37.3	–	9.4	9.3	9.3	9.3±0.7
Ponte Brolla	zircon	Bern-18	12	1149	57.0	1465	72.6	–	19.3	18.3	18.9	18.9±0.9
KAW 2103	apatite	Bern-14	–	266	0.989	3504	19.7	–	10.1	10.0	10.1	10.1±0.8
Golino	zircon	Bern-16	10	559	54.0	697	67.4	–	19.1	18.9	18.4	18.8±1.2
KAW 2102	apatite	Bern-14	–	71	0.120	345	1.94	–	12.4	12.3	12.3	12.4±1.7
Arcegno	zircon	Bern-16	10	795	54.6	975	67.0	0.807	19.2	19.0	18.5	18.9±1.5
KAW 2105	apatite	Bern-19	10	118	1.45	3006	37.0	0.0395	15.0	15.3	15.2	15.2±2.1
Porto Ronco	zircon	Bern-17	11	598	86.7	289	41.9	–	48.5	47.9	48.0	48.2±3.7
72N8-3 Fish Canyon Tuff	zircon	Bern-16	10	1256	54.3	1112	48.1	–	26.9	26.6	25.9	26.5±1.3
FCZ-66d	zircon	Bern-17	10	1319	47.4	1063	38.2	–	29.1	28.8	28.9	28.9±1.4

et al. 1983). Only tracks parallel or sub-parallel to the polished surface were measured to ensure determination of the full track length.

Zircon was analysed using the EDM (Gleadow 1981) with spontaneous tracks being counted in the zircon crystals and induced tracks in an external detector of low uranium mica, held in close contact with the zircons during irradiation. Zircons were mounted in FEP-Teflon, polished and etched in a NaOH-KOH eutectic at 220° C for 24 h (Gleadow et al. 1976). Mica detectors were etched after irradiation to reveal induced tracks using 40% HF at 20° C for 40 min. Track densities were determined at a nominal magnification of 1250 using an oil-immersion objective, with zircons being strictly selected: only prismatic sections parallel to the c-crystallographic axis were used, having sharply etched polishing scratches and with well-etched tracks in all directions. For such crystals, a geometry factor of 0.5 is appropriate (Gleadow and Lovering 1977; Naeser et al. 1980).

All thermal neutron irradiations were carried out in the J1 facility of the Herald reactor, Aldermaston, UK (Hurford and Green 1983). Neutron fluences were monitored by counting induced tracks in etched muscovite detectors against three uranium dosimeter glasses SRM 612, CN-1 and CN-2 (Hurford and Green

Table 3. Counting data for dosimeter glass micas used for FTD irradiations

Irradiation	SRM 612		CN−1		CN−2	
	N_d	ϱ_d ($\times 10^5$ tcm^{-2})	N_d	ϱ_d ($\times 10^5$ tcm^{-2})	N_d	ϱ_d ($\times 10^5$ tcm^{-2})
FTD-113	2134	1.198	3855	3.245	7071	3.001
Bern-4	2210	1.240	4604	3.875	4156	3.498
Bern-6	1260	1.343	5157	4.341	4859	4.090
Bern-7	2576	1.446	4915	4.137	4804	4.044
Bern-9	3245	1.366	4968	4.182	4444	3.741
Bern-10	7548	6.354	5487	18.48	5352	18.02
Bern-14	3687	6.207	6521	18.30	6094	17.10
Bern-16	3363	1.415	4965	4.179	4521	3.806
Bern-17	3314	1.395	4900	4.125	4593	3.866
Bern-18	3470	1.460	4932	4.152	4826	4.062
Bern-19	6693	22.54	4090	68.86	3788	63.77

1982). FT ages of apatites and zircons have been calculated using the zeta calibration approach (Fleischer and Hart 1972; Hurford and Green 1982) whereby a calibration baseline factor zeta is derived for each dosimeter glass by repeated dating analyses of mineral age standards. Only by using such an approach can the problem of "choosing" a value for the ^{238}U spontaneous fission decay constant λ_f and the complexities of neutron dosimetry be avoided. Values of zeta for zircon and apatite have been determined for each of these three dosimeter glasses (Hurford and Green 1983, and Table 2) permitting calculation of ages for the Maggia samples by reference to each glass, thus providing a control on the internal consistency of the 3 neutron dosimeters. Errors have been calculated from Poissonian statistics (the conventional error of Green 1981) together with an uncertainty on the zeta calibration factor.

As a control of calibration and technique, mounts of the Fish Canyon Tuff zircon standard were included in two of the irradiations.

K/Ar dating. K/Ar age analyses were made on separated biotite and muscovite concentrates. Potassium was determined using a Beckmann flame photometer (Purdy and Jäger 1976), two sample

Table 4. K/Ar analytical data for Maggia samples

Sample and locality	Mineral and fraction		K%	$^{40}Ar_{rad}$ ($\times 10^{-6}$) cm^3 (STP)g	$^{40}Ar_{rad}$ (%)	Age (Ma) ($\pm 1\sigma$)
KAW 1877	biotite	50/80	7.44	4.486	70.42	15.4±0.2
Lago Bianco	muscovite	50/80	8.81	5.776	73.45	16.8±0.2
KAW 1876	biotite	50/80	7.91	4.385	81.69	14.2±0.2
Val Bavona	muscovite	60/80	8.86	5.757	79.80	16.6±0.3
KAW 1887	biotite	80/100	7.78	4.829	84.80	15.9±0.2
Menzonio	muscovite	80/100	8.52	5.700	85.45	17.2±0.2
KAW 1878	biotite	80/100	7.72	4.646	79.74	15.4±0.2
Bosco Gurin	muscovite	80/100	9.04	5.694	74.57	16.1±0.2
KAW 1881 Linescio	biotite	80/100	7.72	4.420	66.14	14.7±0.2
KAW 1886 Riveo	biotite	80/100	8.01	4.763	79.80	15.2±0.2
KAW 1885	biotite	80/100	7.60	4.841	77.85	16.3±0.2
Giumaglio-Someo	muscovite	80/100	8.60	6.200	87.63	18.5±0.2
KAW 1879 Valle Vergeletto	biotite	60/80	7.64	5.242	78.69	17.6±0.2
KAW 2099 Maggia	biotite	60/80	7.33	5.118	91.08	17.9±0.2
KAW 1880 Valle Onsernone	biotite	60/80	8.01	5.893	90.23	18.8±0.2
KAW 1884	biotite	80/100	7.40	5.005	83.31	17.3±0.2
Moghegno	muscovite	80/100	8.88	6.408	90.33	18.5±0.2
KAW 2100	biotite	60/80	7.26	5.486	90.26	19.3±0.2
Ronchi	muscovite	60/80	8.66	6.584	75.66	19.5±0.2
KAW 2104 Cima della Trosa	biotite	60/80	7.36	5.876	87.17	20.4±0.3
KAW 1882 Intragna	biotite	80/100	7.85	5.721	88.17	18.6±0.2
KAW 2101	biotite	60/80	7.54	5.999	90.36	20.4±0.2
Ponte Brolla	muscovite	60/80	8.59	6.992	87.05	20.8±0.2
KAW 1883	biotite	80/100	7.93	5.903	82.54	19.0±0.2
Ponte Brolla (pegmatite)	muscovite	80/100	8.89	6.694	85.91	19.3±0.3
KAW 2103	biotite	60/80	7.83	5.939	90.56	19.4±0.2
Golino	muscovite	60/80	8.55	6.866	78.92	20.5±0.2
KAW 2102 Arcegno	biotite	60/80	7.28	6.053	80.35	21.3±0.2
KAW 2105	biotite	60/80	7.43	5.478	98.79	180 ±2
Porto Ronco	muscovite	80/100	8.54	5.775	97.71	166 ±2

Table 5. Rb/Sr analytical data for Maggia samples. (Note: mica ages are calculated using the whole-rock $^{87}Sr/^{86}Sr$ ratio)

Sample and locality	Mineral and fraction		Rb total ppm	Sr total ppm	^{87}Sr rad	$^{87}Sr/^{86}Sr$	$^{87}Rb/^{86}Sr$	Age (Ma) ($\pm 1\sigma$)
KAW 1877	whole-rock		111.6	151.6	0.1089	0.7172	2.131	
Lago Bianco	biotite	35/50	394.6	7.536	0.02949	0.7500	152.1	15.4±0.2
	muscovite	50/80	240.9	51.88	0.05556	0.7209	13.45	22.5±1.9
KAW 1876	whole-rock		207.0	83.37	0.1503	0.7284	7.198	
San Carlo	biotite	50/80	836.3	4.457	0.05164	0.8297	549.4	13.2±0.2
	muscovite	60/80	432.5	9.054	0.04808	0.7645	138.9	19.3±0.3
KAW 1887	whole-rock		122.8	236.9	0.06386	0.7126	1.500	
Menzonio	biotite	80/100	681.2	4.818	0.04415	0.8045	413.0	15.7±0.2
	muscovite	80/100	401.3	32.9	0.03612	0.7211	35.34	17.6±2.1
KAW 1878	whole-rock		312.1	70.33	0.3867	0.7664	12.91	
Bosco Gurin	biotite	40/80	1542.1	1.963	0.09759	1.245	2393.0	14.2±0.2
	biotite	80/100	1578.7	1.396	0.1004	1.502	3526.8	14.7±0.2
	muscovite	80/100	788.3	7.496	0.09643	0.8431	308.3	18.3±0.3
KAW 1881	whole-rock		93.18	417.7	–	0.7085	0.6456	
Linescio	biotite	80/100	476.6	3.596	0.02870	0.7922	386.7	15.3±0.3
KAW 1886	whole-rock		102.8	463.1	–	0.7091	0.6423	
Riveo	biotite	60/80	445.3	3.024	0.02958	0.8109	430.3	16.7±0.2
	biotite	80/100	453.6	4.805	0.02840	0.7707	274.8	15.8±0.3
KAW 1885	whole-rock		93.55	247.1	0.1693	0.7169	1.096	
Giumaglio-Someo	biotite	60/80	516.7	3.310	0.03550	0.8207	456.6	16.1±0.2
	biotite	80/100	492.0	5.089	0.03555	0.7818	281.8	16.3±0.3
KAW 1879	whole-rock		107.2	285.0	0.01798	0.7105	1.089	
Valle Vergeletto	biotite	35/60	598.7	5.825	0.04441	0.7884	299.7	18.4±0.3
	biotite	60/80	577.0	5.389	0.04397	0.7940	312.4	18.9±0.3
	biotite	80/100	605.0	5.799	0.04432	0.7886	304.3	18.1±0.3
KAW 2099	whole-rock		66.27	364.3	0.05187	0.7116	0.5265	
Maggia	biotite	60/80	756.0	10.16	0.07103	0.7821	216.8	23.0±0.3
KAW 1880	whole-rock		117.8	271.2	–	0.7090	1.257	
Valle Onsernone	biotite	35/60	516.1	2.714	0.03976	0.8619	558.5	19.3±0.2
	biotite	60/80	512.7	3.499	0.03916	0.8256	428.7	19.2±0.3
	biotite	80/100	503.1	4.418	0.03885	0.8006	332.4	19.5±0.3
KAW 1884	whole-rock		77.85	353.8	0.01035	0.7102	0.6368	
Moghegno	biotite	100/150	729.6	7.741	0.05301	0.7807	274.7	18.1±0.3
	muscovite	100/150	410.9	80.92	0.03110	0.7141	14.70	19.6±0.6
KAW 2100	whole-rock		41.86	425.1	–	0.7080	0.2849	
Ronchi	biotite	60/80	377.8	9.305	0.02631	0.7392	117.8	18.7±0.2
	muscovite	60/80	229.2	60.44	0.01008	0.7119	10.98	26.0±0.9
KAW 2104	whole-rock		86.25	349.3	–	0.7079	0.7145	
Cima della Trosa	biotite	60/80	472.8	10.85	0.03581	0.7440	126.5	20.2±0.3
KAW 1882	whole-rock		149.3	215.5	0.09657	0.7145	2.013	
Intragna	biotite	60/80	848.1	4.558	0.06918	0.8675	546.8	19.8±0.3
	biotite	80/100	839.8	4.956	0.06597	0.8478	497.0	19.0±0.3
KAW 2101	whole-rock		159.4	126.2	0.09282	0.7177	3.658	
Ponte Brolla	biotite	60/80	698.1	3.398	0.05639	0.8827	604.6	19.3±0.2
	muscovite	60/80	387.4	15.54	0.04689	0.7411	72.34	24.0±0.5
KAW 1883	whole-rock		310.0	27.35	0.3075	0.8261	33.17	
Ponte Brolla	biotite	60/80	2279.0	1.464	0.1928	2.261	5190.0	19.6±0.2
	biotite	<100	2260.0	1.721	0.1901	1.979	4283.0	19.1±0.2
	muscovite	80/100	1443.0	2.750	0.1567	1.328	1610.0	22.4±0.2
KAW 2103	whole-rock		74.19	581.2	0.1173	0.7122	0.3695	
Golino	biotite	60/80	550.5	7.733	0.04389	0.7685	207.2	19.2±0.2
	muscovite	60/80	253.6	81.84	0.03885	0.7150	8.973	22.9±1.0
KAW 2102	whole-rock		178.6	179.1	0.1194	0.7170	2.889	
Arcegno	biotite	60/80	830.0	6.916	0.03288	0.7590	349.0	8.6±0.1
KAW 2105	whole-rock		102.9	69.60	0.1861	0.7376	4.289	
Porto Ronco	biotite	60/80	502.4	4.553	0.3297	1.508	344.2	160 ±2
	muscovite	80/100	209.6	37.15	0.2268	0.7730	16.43	205 ±4

Appendix 1 (Table 5)

KAW 1877 Lago Bianco; Grid Ref. 683.300/145.080; road cutting between Robiei and Lago di Cavagnoo; finely banded two-mica gneiss.

KAW 1876 Val Bavona, San Carlo; Grid Ref. 684.040/140.450; roadcut; two-mica gneiss from the Antigorio nappe.

KAW 1887 Menzonio; Grid Ref. 692.700/134.950; cliff face; massive two-mica gneiss.

KAW 1878 Bosco Gurin; Grid Ref. 680.780/130.260; light coloured, platey two-mica gneiss.

KAW 1881 Linescio, Ponte Asciutto; Grid Ref. 688.550/129.550; massive felsic biotite gneiss.

KAW 1886 Riveo; Grid Ref. 691.100/128.500; massive quarries; massive dark biotite-rich gneiss.

KAW 1885 Giumaglio Someo; Grid Ref. 695.050/126.200; roadcut; two-mica granite gneiss.

KAW 1879 Valle Vergeletto, Alla Ca; Grid Ref. 687.900/120.600; fine banded biotite-rich gneiss.

KAW 2099 Maggia; Grid Ref. 697.300/123.150; disused quarry; felsic fine banded gneiss.

KAW 1880 Valle Onsernone, between Vocaglia and Crana; Grid Ref. 689.600/117.600; massive-biotite rich gneiss.

KAW 1884 Moghegno; Grid Ref. 698.400/121.700; from excavation for a new bridge; massive felsic granular gneiss.

KAW 2100 Ronchi; Grid Ref. 699.925/119.425; 5 m roadcut SE of Ronchi; steeply dipping felsic two-mica gneiss.

KAW 2104 Cima della Trosa; Grid Ref. 704.325/118.538; outcrop of biotite-rich, equigranular gneiss at summit (1,870 m); dipping 85° N.

KAW 1882 Intragna; Grid Ref. 697.200/115.150; old quarry; biotite-rich banded gneiss.

KAW 2101 Ponte Brolla; Grid Ref. 701.650/116.300; small quarry N of Ponte Brolla; fine-banded two-mica gneiss, dipping 80° N.

KAW 1883 Ponte Brolla; Grid Ref. 701.330/115.800; massive pegmatite outcrop in river.

KAW 2103 Golino; Grid Ref. 699.375/114.775; 15 m roadcut E of Golino; two-mica, coarse augen gneiss dipping 80° N; mylonitised gneiss within 50 m of sample.

KAW 2102 Arcegno; Grid Ref. 700.050/113.300; 10 m cliff face, W of Arcegno; metavolcanic with prominent feldspar phenocrysts dipping 65° N.

KAW 2105 Porto Ronco; Grid Ref. 699.463/110.750; excavation for a new building; two-mica finely-banded gneiss, dipping 30° N.

solutions of different concentration giving results agreeing to better than $\pm 1\%$. For the argon analyses 0.1 to 0.2 g aliquots of mineral were fused using an RF generator and the evolved gases passed through a 2-stage purification system using Ti and Cu/CuO getters in a quartz/pyrex-glass line (Flisch 1982). Isotopic ratios were measured with a MM 1200 mass spectrometer in static mode, employing an enriched ^{38}Ar spike (Schumacher 1975) calibrated against both known air volumes and the standard minerals B-4M, B-4B, LP-6 and GL-0 (Flisch 1982). Blank values for ^{40}Ar of $3.2\text{–}5.2 \times 10^{-8} cm^3$ and a mean value of 300.63 for the $^{40}Ar/^{36}Ar$ air ratio were measured before and between the sample analyses. Potassium and argon analyses of the standard minerals B-4B and B-4M were interspersed with the Maggia samples as a control of experimental technique and spike calibration. Errors on measured ages were calculated according to the error propagation of Gaussian Law, combining individual uncertainties from potassium analysis, weighing, argon isotopic ratios and spike calibration.

Rb/Sr dating. Biotite, muscovite and whole-rock samples were prepared using the procedures of Jäger (1979) with initial semi-quantitative determination of Rb and Sr by X-ray fluorescence analysis. Sr and Rb were analysed by isotope dilution using ^{87}Rb and ^{84}Sr spikes. Isotopic ratios were measured using a 35 cm radius Ion Instruments solid source mass spectrometer fitted with a triple filament source linked to a Keithley 642 amplifier and Prema 6040 digital voltmeter. Data acquisition was via a PDP-11 computer. Uncertainty on the $^{87}Sr/^{86}Sr$ ratio is $\sim 0.02\%$ and on the $^{87}Rb/^{86}Sr$ ratio $\sim 1\%$. Consistency of analysis was assessed by determination of NBS 987 $^{87}Sr/^{86}Sr$ ratios throughout the measurement period, giving a mean value of 0.710103 ± 27 (1σ; n = 30).

All ages have been calculated using IUGS recommended constants (Steiger and Jäger 1977).

Analytical results

Table 1 shows 96 new radiometric ages determined for the Central Swiss Alps using 3 dating methods on 4 different minerals. FT count data for 18 apatite and zircon samples from the Maggia Valley, and 2 Fish Canyon Tuff zircon standards are presented in Table 2. Ages calculated by reference to each dosimeter glass are shown together with the mean age; all errors are 1σ. For apatite population analyses a minimum of 100 crystals were counted for each of the spontaneous and induced measurements. The paucity of spontaneous tracks in most samples results from both low uranium content and low age and is reflected in the high errors on the calculated ages, a mean of $\pm 9\%$ at the 1σ level. EDM analyses were subjected to the χ^2 test (Galbraith 1981) to detect whether the results contained any extra-Poissonian scatter: where the analysis failed the χ^2 test, the age was calculated with the mean individual crystal ϱ_s/ϱ_i ratio, $\overline{(\varrho_s/\varrho_i)}$, which gives approximately the same age but makes allowance for the wider spread of individual crystal values. 1σ errors on FT zircon ages are typically $\pm 6\%$. Table 3 details the dosimetry data from the 3 uranium glasses SRM 612, CN-1 and CN-2 for the pertinent irradiations. No apatite was recovered from sample KAW 1883 whilst the zircon was found to be metamict.

Apatite FT ages published previously for Alpine samples (Wagner and Reimer 1972; Schaer et al. 1975; Wagner et al. 1977) have utilized a calibration based on a λ_f value of $8.42 \times 10^{-17} a^{-1}$ and neutron dosimetry via a moldavite glass calibrated initially against cobalt activation monitors (Wagner 1969). The broad similarity of apatite ages in the present study with those determined previously in the Ticino area (see Wagner et al. 1977, Map 1) suggests comparability within error limits.

Table 4 details the analytical results of K/Ar analyses on 19 biotite and 11 muscovite separates from Maggia samples. All errors are 1σ and typically $\pm 1.5\%$. Excepting the Ivrea sample, Maggia biotite ages range between 14 and 21 Ma, muscovite ages between 16 and 21 Ma.

Rb/Sr analytical data for 19 whole-rock and biotite samples and 10 muscovite separates from Maggia rocks are listed in Table 5. Errors are 1σ. For 7 samples, biotite from more than one size fraction was analysed as a test of reproducibility: in each case measured ages from different size fractions are in good agreement within 2σ error limits. Mica ages are corrected using the $^{87}Sr/^{86}Sr$ value measured for the whole-rock sample, which makes the assumption of strontium homogenisation between minerals within the total rock system during Alpine metamorphism (Jäger 1970). In a slowly cooled rock, the correction of biotite ages strictly should use the $^{87}Sr/^{86}Sr$ ratio of the whole-rock minus the white mica phase, since white mica is closed to strontium before the biotite closure temperature is reached. For these Maggia samples, the assumption of whole-rock

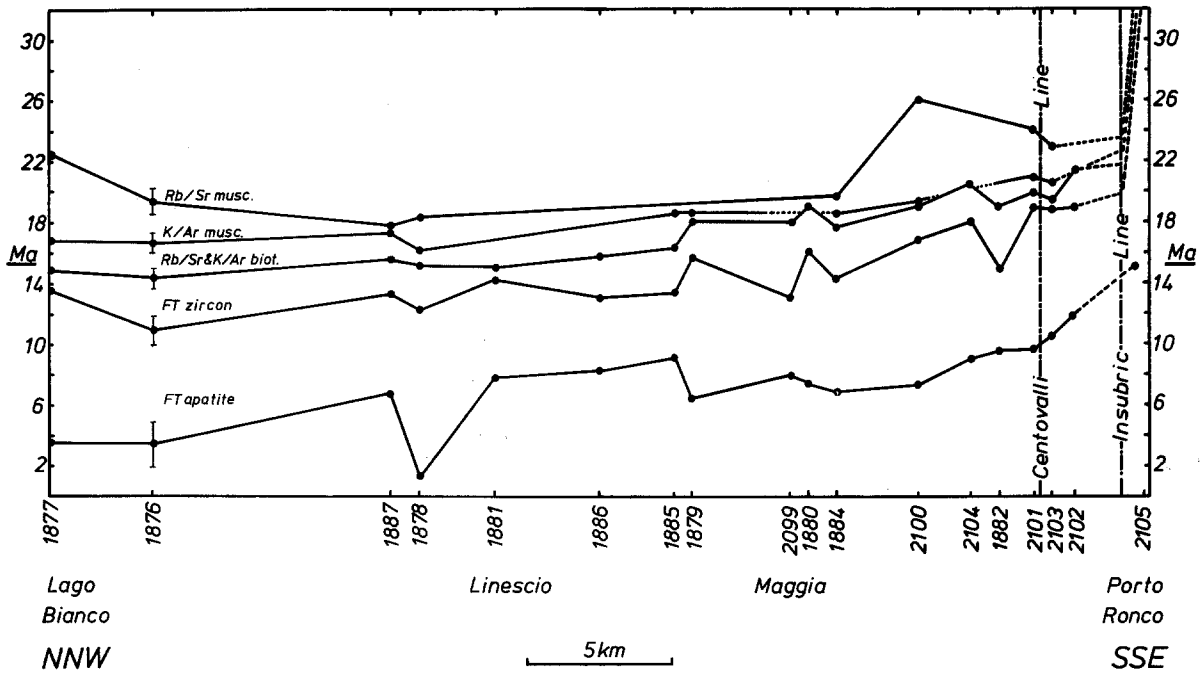

Fig. 2. Graphical representation of measured mineral ages along the Maggia Valley profile. 2σ error bars are typical of each age. Apatite ages are recalculated to a common altitude of 350 m

$^{87}Sr/^{86}Sr$ initial ratios for biotite introduces negligible errors, well within the 1σ uncertainties quoted for the calculated ages.

Figure 2 shows offers a graphical representation of the measured ages: the different mineral ages for each sample are plotted along the profile from NNW to SSE. 2σ error bars are shown typical of each age. For each mineral-isotopic system there is, within analytical error, reasonable uniformity of age in the northern half of the section, as far south as Someo-Maggia: FT apatite gives a mean age of ~6 Ma (recalculated to a common altitude of 350 m – see below), approximating to the 2 published apatite ages in the adjacent Valley Verzasca (Wagner et al. 1977). Apatite from sample KAW 1878 at Bosco Gurin gave a very young age, at variance with results from adjacent samples: no explanation of this anomaly is at present apparent. FT zircon gives a mean of ~13 Ma, biotite a mean age of ~15 Ma, confirming the single analysis from Riveo (Purdy and Jäger 1976) and the Verzasca Valley (Jäger et al. 1969). K/Ar muscovite ages average 16–17 Ma in the northern Valley, with Rb/Sr muscovite ages at 22.5 Ma in the north, dropping to 18 Ma mid-Valley, substantiating previous limited determinations (Jäger et al. 1967). The Pennine steep-belt is entered south of Maggia-Moghegno and a gradual increase is seen in each mineral age system. In the immediate vicinity of the Centovalli line there is a strong grouping of zircon and mica ages between 19 and 24 Ma. The Porto Ronco sample from the Ivrea zone gives Prealpine mica ages, 48 Ma for FT zircon and 15 Ma for FT apatite.

Figure 3 shows the distributions of confined fission track lengths measured in apatite for samples along the profile. The mean spontaneous track length and pattern of length distribution can be diagnostic of cooling rate and reveal low temperature thermal effects (Gleadow et al. in prep.). Excepting KAW 1877, 1884 and 2099, for which small numbers of tracks were measured, each sample reveals a unimodal distribution, with mean track lengths between 11.7 and 13.7 μm. No distinction can be made between samples in different areas of the profile, suggesting a similar style of cooling through the apatite annealing zone. The overall mean length of 12.7 ± 0.7 μm ($\pm 1\sigma$) lies within the range of 12–14 μm found for more than 150 slowly cooled plutonic rocks, significantly shorter than the range of 14–15 μm found for fast cooling volcanic rocks (Gleadow et al. in prep.).

Discussion

Cooling curves and closure temperature considerations

For each sample the sequence of measured ages FT apatite < FT zircon < K/Ar biotite ≅ Rb/Sr biotite < K/Ar muscovite < Rb/Sr muscovite is consistent with the range of assumed system closure temperatures (Purdy and Jäger 1976; Wagner et al. 1977; Harrison and McDougall 1980; Dempster 1985) below which the daughter product is retained. Thus the ages measured in this study probably represent cooling ages subsequent to some phase of Alpine metamorphism. Thermal models for cooling have been constructed for each sample (Figs. 4, 5, 6) by plotting measured mineral ages against assumed closure temperatures (see Wagner et al. 1977; Harrison et al. 1979).

Closure temperatures for retention of tracks in apatite are defined by both extrapolation of laboratory annealing experiments to geological time (Wagner 1968; Naeser and Faul 1969) and from borehole samples where increase in depth and temperature produces a decrease in age (Naeser 1979; Gleadow and Duddy 1981). Over geological time (10 Ma) tracks in apatite begin to anneal around 70° C with complete track loss at ~125° C. These low closure temperatures are sensitive to the time spent in the track annealing zone and thus to the rate of cooling. For faster rates of cooling, as in uplifting mountain belts, a value of 115–120° C has been proposed by Wagner et al. (1977) and

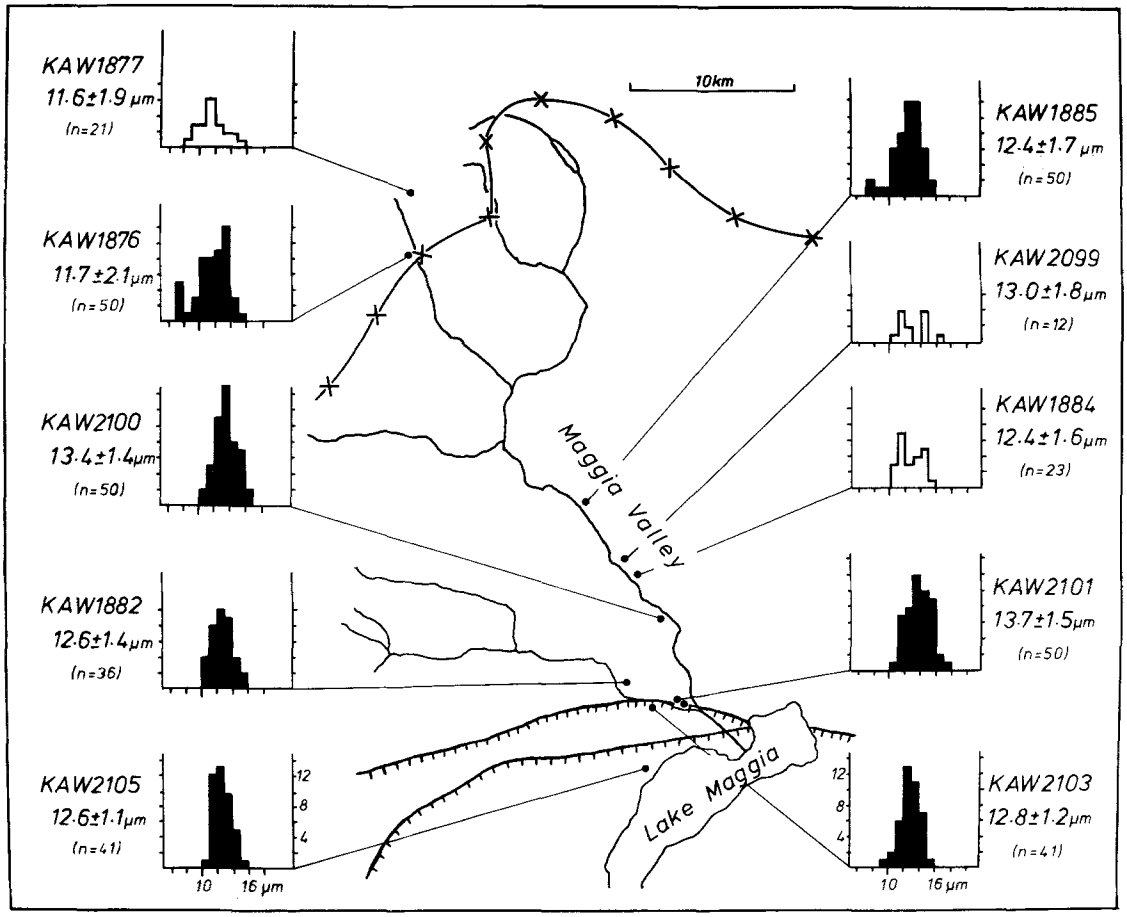

Fig. 3. Distributions and mean values of confined FT lengths in apatite from Maggia Valley samples. Distributions shown in outline represent small numbers of measured track lengths

Zeitler et al. (1982), although Haack (1977) has calculated the slightly lower value of 94° C for a cooling rate of 10° C/Ma. For fission tracks in zircon, similar extrapolation of annealing experiments suggests closure temperatures >300° C (Fleischer et al. 1965; Krishnaswami et al. 1974) whilst limited geological evidence favours a lower temperature 175–250° C (e.g., Gleadow and Brooks 1979; Harrison et al. 1979; Zeitler et al. 1982).

The closure temperature for the retention of argon and strontium in biotite is a contentious subject: Wagner et al. (1977) derived a value of 300±50° C from the coincidence of reset Prealpine K/Ar and Rb/Sr biotite ages with the stilpnomelane metamorphic isograd in the Lepontine Alps. Such a value is supported by a tectonothermal argument from Dallmeyer (1978) 300–345° C, whilst contact metamorphic studies support >300° C (Hanson and Gast 1967) and argon diffusion studies give 280±40° C (Harrison and McDougall 1980). Turner and Forbes (1976) proposed ~225° C from the extreme extrapolation of limited borehole data, whilst Berger and York (1981) obtain 350–400° C from argon diffusion experiments. Verschure et al. (1980) propose 400° C (or higher) because of the retention of a 870 Ma Sveconorwegian age by a brown biotite despite the growth of green Caledonian biotite. The concordance of Rb/Sr and K/Ar biotite ages in slow cooling terrains (this study Table 1; Purdy and Jäger 1976; Siegenthaler 1984 and references therein; Dempster 1985) underlines the similarity of closure temperature for the two systems. Clearly a unique closure temperature for biotite is unlikely: the relevance of the Alpine derived value favours the use of 300±50° C in this study.

500±50° C for the closure temperature for strontium in muscovite hails from the relation of Alpine/Prealpine muscovite ages to the staurolite/chloritoid transition in the Lepontine Alps (Wagner et al. 1977), whilst a closure temperature of 350° C for argon in muscovite represents an extrapolation between biotite and Rb/Sr muscovite (Purdy and Jäger 1976).

Figure 4 shows a cooling curve for a single sample KAW 1884 from Moghegno, which illustrates that a closure temperature for the FT zircon system may be assessed relative to the closure temperatures for other mineral – isotope systems from the intercept of the measured zircon age with the cooling curve. Figure 5 shows the cooling patterns of 18 samples divided into 3 groups:

(i) northern and central Maggia Valley, with sub-horizontal gneisses,
(ii) southern Maggia Valley from Moghegno to Ponte Brolla, a transition zone where effects of Neoalpine deformation are detectable and
(iii) the Southern Steep Belt, including samples adjacent to the Centovalli fault line, but north of the Insubric mylonites.

A mean closure temperature of 240±50° C for the retention of fission tracks in zircon is derived from the cooling curves in Fig. 5 (17 samples, ±2 standard errors of the mean).

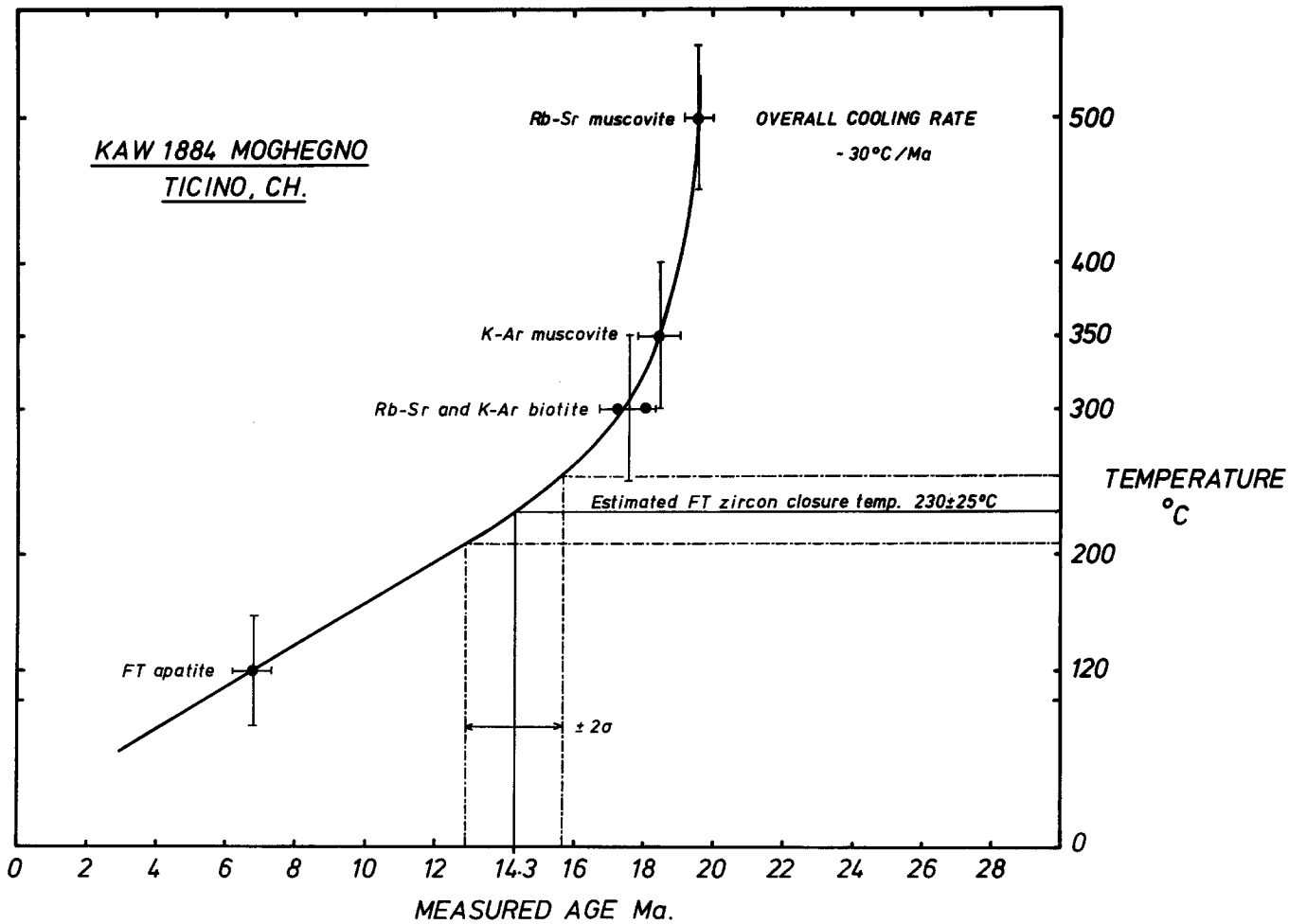

Fig. 4. Cooling curve for sample KAW 1878 from Bosco Gurin, plotted from measured mineral ages against assumed system closure temperatures. Fig. 4 illustrates how a FT zircon closure temperature is estimated from the intercept of measured age with the curve

The cooling curve for the single Ivrea zone sample is shown in Fig. 6. Initial cooling (500–300° C) in Mid Jurassic times confirms the pattern suggested by Zingg (1983 and references therein) and interpreted as the superposition of thermal activity from the breakup of the continental margin upon Variscan cooling. Apparent thermal quiescence throughout the Cretaceous was followed by very slow cooling through the Tertiary, with cooling rates of around 8° C/Ma over the last 15 Ma.

Late Oligocene to Recent thermal history and uplift pattern: an interpretation

In an iterative attempt to refine the cooling patterns, Fig. 7 presents 3 cooling paths, representing the mean of each area north of the Insubric Line (Fig. 5) and including the 240° C FT zircon geochronometer. The paths are extended to the present day, assuming an arbitrary mean temperature value of 10° C; analytical errors on determined ages and uncertainties on closure temperatures swamp any correction to present-day temperatures resulting from geomorphological constraints. The results in Fig. 7 must be considered with respect to these errors and uncertainties which although affecting their absolute accuracy, apply equally to all points, and thus relative differences of cooling paths are probably real.

The 3 subareas north of the Insubric Line exhibit roughly similar cooling patterns, each with continuous cooling since the Late Oligocene – Early Miocene at overall rates of between 20 and 26° C/Ma. In each subarea, a time interval of accelerated cooling is succeeded by a slower rate of cooling between 11 and 17° C/Ma for the Late Miocene to present, recent cooling probably resulting from uplift induced by isostatic adjustment (Neugebauer et al. 1980). The accelerated cooling rates of 50–80° C/Ma during the time interval 23–16 Ma may result from some uplift other than the isostatic readjustment considered for the Late Miocene to present. Comparison of the cooling curves (Fig. 7) reveals progressively earlier cooling to the south: the high rate of cooling occurred in the southernmost area between 23 and 19 Ma, in the northernmost area between 19.5 and 16 Ma. Within the Southern Steep Belt area the cooling curves are not obviously affected by the Centovalli fault line, suggesting that vertical displacements along this branch of the Insubric Line are absent or minor. The impressive difference in the cooling curves of the Ivrea zone (Fig. 6) and the Lepontine Alps (Fig. 5) may possibly be ascribed to vertical displacement within the Insubric mylonite belt. An independent structural analysis (Schmid et al. in press) has shown that the steeply N-dipping Insubric mylonite belt accommodates a backthrusting motion of the Central Alps over the Southern Alps. It is conceivable that

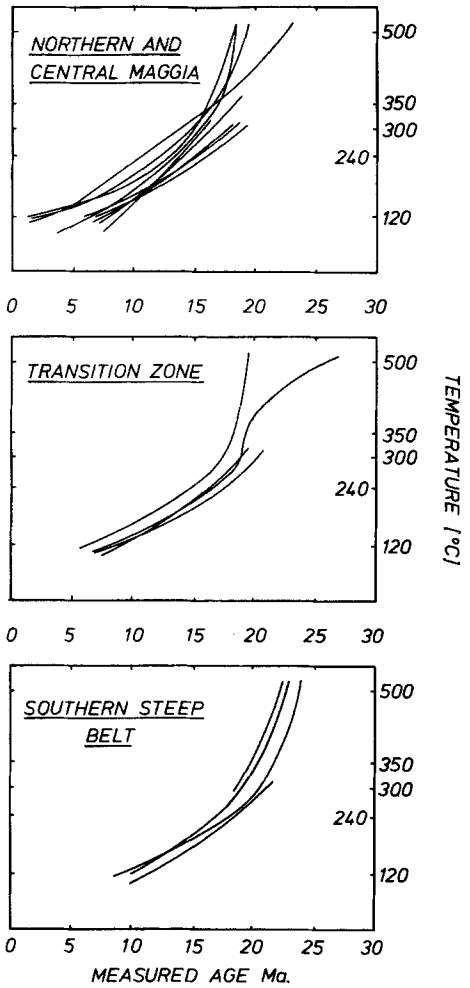

Fig. 5. Combined cooling curves from samples north of the Insubric Line divided into 3 tectonic areas as described in text. A FT zircon closure temperature has been estimated from each curve, giving a mean value of $240 \pm 50°$ C

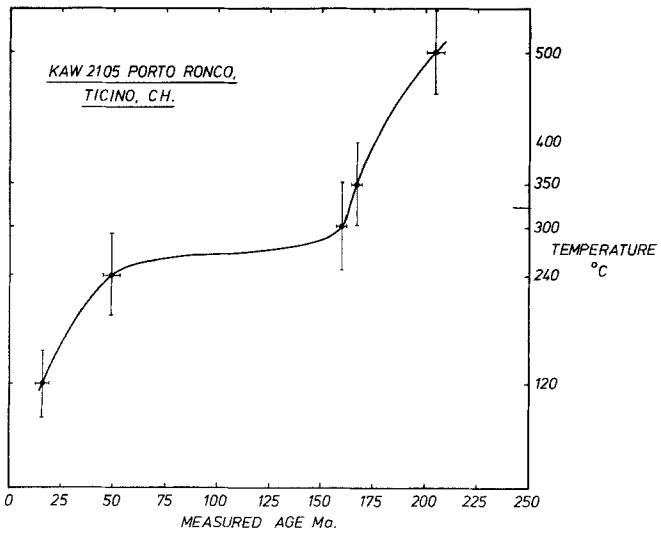

Fig. 6. Cooling curve for Ivrea Zone sample KAW 2105 from Porto Ronco

the period of rapid cooling of the Lepontine Alps, from 23–16 Ma, results from uplift and backthrusting during active Neoalpine crustal shortening, rather than from passive isostatic adjustment.

Schmid et al. (1986) consider the formation of the Southern Steep Belt as contemporaneous with the backthrusting of the Central Alps along the mylonite belt. The drift northwards towards younger ages of rapid cooling may be interpreted tentatively in terms of a time lag between a fixed time of rapid uplift associated with backthrushing, and the time of rapid cooling. 23 Ma may therefore represent a minimum age for the onset of backthrusting and Steep Belt formation, since the timing is artificially constrained by the 500° C maximum chronometer in Fig. 7. As parts of the Bergell batholith are affected by the schistosity within the Southern Steep Belt (Heitzmann 1975; Vogler and Voll 1981), the backthrusting must postdate the intrusion of the Bergell granite at around 30 Ma (Gulson 1973; Deutsch and Steiger 1985).

Conversion of cooling rates to uplift rates requires independent estimates of both the geothermal gradient and possible changes in the geothermal regime, such as the relaxation of geotherms following tectonism. However from a comparison of FT apatite ages measured for rocks at different elevations, an uplift rate may be calculated directly without assumptions about the geothermal gradient. The low closure temperature for the retention of fission tracks in apatite renders it sensitive to recent uplift through the track annealing zone, broadly equivalent to uplift through the $120 \pm 20°$ C isotherm and thus, for a limited lateral distance, uplift rates may be calculated directly from comparison of differences in age and altitude. At the southern end of the profile a vertical difference of 1,619 m between Cima della Trosa and Ponte Brolla (lateral distance of 2,000 m) equates with a FT apatite age difference of 3.6 Ma, indicating an uplift rate of 0.45 mm/a for the Late Neogene-Quaternary. This uplift rate compares well with previous estimates of isostatic uplift in the Ticino area around 0.4 mm/a (Wagner et al. 1977) and in the Alps in general 0.4–1 mm/a (Clark and Jäger 1969; Wagner and Reimer 1972; Schaer et al. 1975) and is consistent with precision levelling measurements which indicate a maximum uplift rate of 1 mm/a (e.g., Jeanrichard 1975). Because of this demonstrable dependency of apatite age upon sample elevation, apatite ages in Tables 1 and 2 are shown recalculated to a single elevation of 350 m, the mean height of the Maggia Valley floor, (assuming a similar uplift rate of 0.4 mm/a for all samples), thus permitting direct comparison of results from different samples. Note that mica and FT zircon ages from Cima della Trosa and Ponte Brolla are identical within error, indicating that an altitude dependency is not discernible for these systems.

In another approach, Werner (1980) has proposed a model of an uplifting body, the Central Alps, juxtaposed to a resting body, the Southern Alps, the two bodies being separated by a vertical fault, the Insubric Line. For a rock 15 km north of the Insubric Line, a cooling rate of 65–70° C/Ma resulted from uplift rates of 2–3 mm/a over a time interval of about 5 Ma (Figs. 5 and 7 in Werner 1980). This model yields a geothermal gradient of ~27° C/km, tolerably close to a normal gradient of 30° C/km. An independent assessment of the Late Miocene to Quaternary geothermal gradient may be made by dividing the mean cooling rate of 14° C/Ma (derived from measured mineral ages vs assumed closure temperatures, Fig. 7) by the uplift rate of 0.45 mm/a (derived from the gradient of FT apatite age with altitude): 31° C/km again supports the use of a

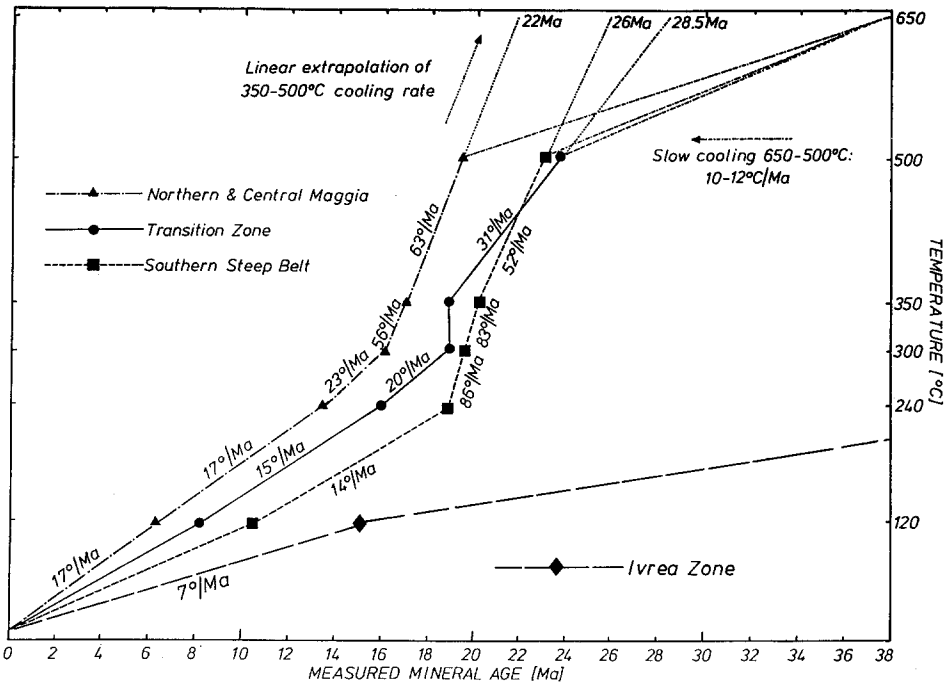

Fig. 7. Mean cooling patterns for the 3 areas north of the Insubric Line. The mean FT zircon closure temperature and measured zircon ages are included in the cooling paths as a refinement of the curves in Fig. 5. Low temperature cooling path of Ivrea Zone sample is included for comparison

normal gradient in the following calculation of 'assumed' uplift rates, although the assumption of constancy of the geotherm through time may be invalid.

For the Steep Belt, the mean cooling rate from 23–19 Ma is 65° C/Ma, equivalent to an uplift rate of ~2.2 mm/a. Maintained over 4 Ma, the minimum period of fast cooling, a minimum uplift of the Lepontine Alps by 9 km is found, possibly by backthrusting along the Insubric mylonites. Late Miocene to Recent cooling in the Steep Belt has a mean rate of 14° C/Ma, which in turn gives an uplift rate of 0.47 mm/a, possibly from isostatic adjustment; maintained over 19 Ma this rate produces an additional uplift of the Lepontine Alps by some 9 km. In contrast, calculation of uplift for the Ivrea zone over a similar total time period, 23 Ma, using the cooling rate of 8° C/Ma obtained above (section 5.1), gives about 6 km overall uplift of the Southern Alps. Metamorphic grades of presently juxtaposed Central and Southern Alps (Frey et al. 1980) indicate maximum temperatures of around 650 and 200° C respectively: persisting with a geotherm of 30° C/km, the temperature difference suggests a differential uplift of the Central Alps by >15 km – a figure also suggested by Trümpy (1975). Additional uplift of the Central Alps may be accomodated in the present model by extrapolating the higher uplift rate above 500° C to an earlier time (Fig. 7): 1 Ma linear back extrapolation provides an additional 2 km of uplift.

On the timing of the Mid Tertiary alpine metamorphism

Results from the present study may contribute to the controversy over the age of the "peak" of Mid Tertiary metamorphism, or the possibility of polyphase Meso- and Neoalpine metamorphism. In principle, Rb/Sr muscovite ages of around 23 Ma could represent cooling ages either shortly after a metamorphic peak of 26 Ma (Deutsch and Steiger 1985) or subsequent to the peak of the Lepontine phase at 38–35 Ma (Jäger 1973). Evidence for the Lepontine phase is afforded by numerous Rb/Sr phengite ages around 38–35 Ma determined in the Western Alps, in particular the Monte Rosa nappe (Hunziker 1969, 1970; Bigioggero et al. 1981), a limited number of ages to the north, east and west of the area of high metamorphic grade (Jäger 1970; Jäger et al. 1969) and more recently within the Suretta nappe (Steinitz and Jäger 1981). Occurrence of these ages outside the Mesoalpine staurolite isograd but within the chloritoid zone provides temperature constraints which indicate that the phengite crystallised near the maximum temperature of Mesoalpine metamorphism and that subsequent temperatures were insufficient to rejuvenate the phengites. Accordingly, 38–35 Ma has been interpreted as dating the peak of the Lepontine Phase of metamorphism, after which continuous cooling occurred. No 38–35 Ma ages have been found within the staurolite isograd of the Lepontine area.

Three schematic models may be forwarded as alternatives to describe the timing of the Lepontine Mid-Tertiary metamorphism (Fig. 8). Model A supposes a linear slow cooling from a climactic metamorphic temperature of ~650° C (Frey et al. 1980 and references therein) at 38 Ma, to 500° C at the ages shown in Fig. 7: 19.5 Ma in northern and central Maggia Valley and 23.5 Ma in the south. The U/Pb monazite ages of Köppel and Grünenfelder (1975, 1978), 22 Ma in the northern and central Lepontine Alps (samples 1, 2, 3, 4, 5 and 8) and ~27 Ma in the south (samples 6 and 7) are thus interpreted as cooling ages, with closure temperatures of ~530° C derived from the intersection of the measured monazite ages with the 650–500° C slow cooling paths (see Fig. 7) – values similar to that proposed by Purdy and Jäger (1976). A possible objection to model A is the very slow cooling rate for the Oligocene, a mean rate of 10–12° C/Ma, less than that resulting from Late Neogene-Quaternary isostatic uplift. The supposition is one of continued deep burial with minimal uplift (and thus erosion) until early Miocene. Heavy molasse deposition took place in the north only from late Oligocene (Chattian) times, which offers some support for a low rate of uplift.

Model B(i) envisages maintenance of the maximum Le-

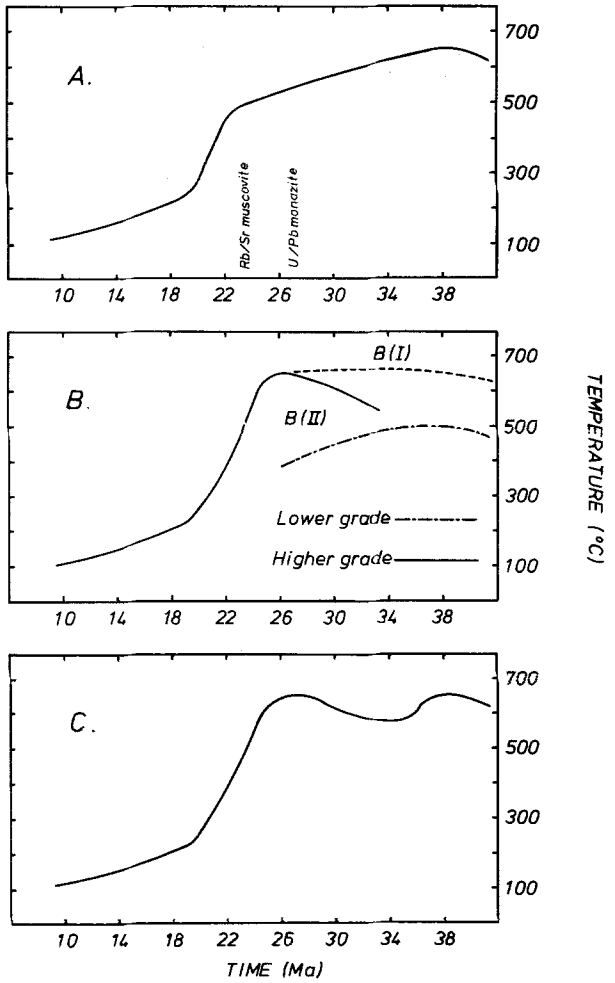

Fig. 8 A–C. Three schematic models for the Mid to Late Tertiary thermal history of the Lepontine Alps

pontine phase temperatures until late Oligocene – early Miocene (28–23 Ma). This is clearly incompatible with the preservation of 38–35 Ma phengite ages in the lower grade, outer margins. Model B(ii) supposes differential heating and cooling patterns for the lower and higher grade areas, with variation between these thermal "end members". Formation of phengites at 38 Ma and $<500°$ C is followed in the lower grade areas by slow cooling. Peak temperatures in the higher grade regions are reached either at 38 Ma and maintained – model B(i) – or, because of slower heating, in the Late Oligocene. The latter hypothesis seems more plausible. Monazite ages can now be interpreted as formation ages, or as cooling ages shortly after formation, $\sim$22 Ma in the central Lepontine and $\sim$27 Ma near the Insubric Line. Linear extrapolation of the 500–350° C cooling paths (Fig. 7) to 650° C indeed suggests ages of $\sim$22 Ma and 28–26 Ma respectively for the two areas. Again this model assumes negligible uplift until late Oligocene. The present level of erosion may reveal higher grade, tectonically deeper rocks in the Central Lepontine, which updomed and cooled later (22–27 Ma), with peripheral, lower grade rocks having cooled at 38–35 Ma.

Model C proposes a post-Lepontine phase of cooling, presumably by uplift, with a second, more restricted metamorphism, synchronous with Neoalpine deformation(s), such as the Steep Belt formation. It is conceivable that the higher grades of metamorphism toward the Insubric Line resulted from a more restricted syn- and postkinematic Neoalpine metamorphism superimposed on Lepontine amhibolite facies event, although the thermal source for such an event is not immediately apparent.

K/Ar hornblende ages (Steiger 1964; Deutsch and Steiger 1985) from the southern and central Lepontine Alps show very considerable scatter between 23.4 and 31.9 Ma plus an actinolite age of 57.1 ± 2.8 Ma. Their conclusion that "the peak of high-grade metamorphism..... which led to the classical mineral zonation pattern concurs with the 23–29 Ma age interval", linked with a generally accepted high, if ill-defined, closure temperature for argon in hornblende tends to give a some support to model B (Fig. 8).

Conclusions

Fission track, K/Ar and Rb/Sr age determinations on a series of samples from the Maggia Valley in the Central Swiss Alps provide new information about the system closure temperature for fission tracks in zircon and cooling and uplift patterns in the Lepontine Alps:

(a) a mean closure temperature of $240 \pm 50°$ C (2σ) is proposed for the retention of fission tracks in zircon, from an extrapolation between measured mineral ages and assumed closure temperatures for Ar and Sr in micas and fission tracks in apatite.

(b) Throughout the late Neogene and Quaternary the entire Maggia Valley profile exhibits a relatively constant cooling rate, between 11 and 17° C/Ma, equated with a mean isostatic uplift of $\sim$0.5 mm/a.

(c) Differences of altitude and FT apatite age independently suggest an uplift of $\sim$0.5 mm/a and confirm the recent geothermal gradient of 30° C/km.

(d) More rapid cooling from higher temperatures occurs earlier in the southern part of the profile.

(e) Assuming a constant, normal geothermal gradient of 30° C/km, uplift rates of $\sim$2.2 mm/a are derived for the Southern Steep Belt area, with total Early Neogene uplift of the Pennine block by more than 9 km, possibly by backthrusting along the Insubric mylonites onto the Southern Alps. The start of this Neoalpine deformation probably predates the onset of rapid cooling in the southernmost area, $\sim$23 Ma, and is tentatively dated at around 27 Ma.

Acknowledgements. I am indebted to Emilie Jäger for initiating and supporting my work in the Maggia and reminding to raise my eyes from problems of calibration to things Alpine; and to Hannes Hunziker for introducing me to Alpine geology and his constant help in the field and lab. Stefan Schmid, André Zingg, Tim Dempster and Andy Gleadow contributed substantially to the preparation of this manuscript. I am grateful to all my colleagues in Berne, particularly Robert Siegenthaler for his computer expertise, Markus Flisch for contructing the argon line, Rolf Brunner for maintaining the mass spectrometers and Hansruedi Steiner for sampling some of the rocks. Garth George, Wilf Sentence and colleagues at Herald provided assistance with irradiations. Geochronological studies in Berne are supported financially by the Schweizerischer Nationalfonds zur Förderung der wissenschaftlichen Forschung.

References

Ayrton SN, Ramsay JG (1974) Tectonic and metamorphic events in the Alps. Schweiz Mineral Petrogr Mitt 54:609–639

Bearth P (1958) Über einen Wechsel der Mineralfazies in der Wurzelzone des Penninikums. Schweiz Mineral Petrogr Mitt 38:363–373

Berger GW, York D (1981) Geothermometry from $^{40}Ar/^{39}Ar$ dating experiments. Geochim Cosmochim Acta 45:795–811
Bernoulli D, Lemoine M (1980) Birth and early evolution of the Tethys: the overall situation. In: Geology of the Alpine Chains born of Tethys. 26th Int Geol Cong Paris
Bigioggero B, Boriani A, Colombo A, Tunesi A (1981) Eta'e caratteri petrochimica degli ortogneiss della zona Moncucco-Orselina nell'area Ossolana. Rendiconti 38:207–218
Clark SP, Jäger E (1969) Denudation rate in the Alps from geochronologic and heat flow data. Am J Sci 267:1143–1160
Dallmeyer RD (1978) $^{40}Ar/^{39}Ar$ incremental release ages of hornblende and biotite across the Georgia Inner Piedmont: their bearing on Late Palaeozoic-Early Mesozoic tectono-thermal history. Am J Sci 278:124–149
Dal Piaz GV, Hunziker JC, Martinotti G (1972) La Zona Sesia-Lanzo e l'evoluzione tettonico-metamorfica delle Alpi nordoccidentali interni. Mem Geol Soc Ital 11:433–460
Dempster TJ (1985) Uplift patterns and orogenic evolution in the Scottish Dalradian. J Geol Soc London 142:111–128
Deutsch A, Steiger RH (1985) Hornblende K/Ar ages and the climax of Tertiary metamorphism in the Lepontine Alps (South Central Switzerland): an old problem reassessed. Earth Planet Sci Letts 72:175–189
Dewey JF, Bird JM (1970) Mountain belts and the new global tectonics. J Geophys Res 75:2625–2647
Fleischer RL, Hart HR (1972) Fission track dating: techniques and problems. In: Bishop WW, Miller JA (eds) Calibration of hominoid evolution. Scott Acad Press, Edinburgh, pp 135–170
Fleischer RL, Price PB, Walker RM (1965) Effects of temperature, pressure and ionization on the formation and stability of fission tracks in minerals and glasses. J Geophys Res 70:1497–1502
Flisch M (1982) Potassium argon analysis. In: Odin GS (ed) Numerical dating in stratigraphy. John Wiley, Chichester, pp 151–158
Frey M, Bucher K, Frank E, Mullis J (1980) Alpine metamorphism along the geotraverse Basel-Chiasso – a review. Eclogae Geol Helv 73:527–546
Galbraith RF (1981) On statistical models for fission track counts. Math Geol 13:471–488
Gansser A (1968) The Insubric Line – a major geotectonic problem. Schweiz Mineral Petrogr Mitt 48:123–143
Gleadow AJW (1981) Fission track dating methods: what are the real alternatives? Nucl Tracks 5:3–14
Gleadow AJW, Brooks CK (1979) Fission track dating, thermal histories and tectonics of igneous intrusions in East Greenland. Contrib Mineral Petrol 71:45–60
Gleadow AJW, Duddy IR (1981) A long-term track annealing experiment for apatite. Nucl Tracks 5:169–174
Gleadow AJW, Lovering JF (1977) Geometry factor for external detectors in fission track dating. Nucl Track Detection 1:99–106
Gleadow AJW, Duddy IR, Lovering JF (1983) Fission track analysis: a new tool for the evaluation of thermal histories and hydrocarbon potential. Austral Petrol Explor Assoc J 23: 93–102
Gleadow AJW, Hurford AJ, Quaife DR (1976) Fission track dating of zircon – improved etching techniques. Earth Planet Sci Letts 33:273–276
Green PF (1981) A new look at statistics in fission track dating. Nucl Tracks 5:77–86
Gulson BL (1973) Age relations in the Bergell region of the South-East Swiss Alps: with some geochemical comparisons. Eclogae Geol Helv 66:293–313
Haack U (1977) The closing temperature for fission track retention in minerals. Am J Sci 277:459–464
Hanson GN, Gast PW (1967) Kinetic studies in contact metamorphic zones. Geochim Cosmochim Acta 31:1119–1153
Harrison TM, McDougall I (1980) Investigations of an intrusive contact, northwest Nelson, New Zealand I: Thermal, chronological and isotopic constraints. Geochim Cosmochim Acta 44:1985–2003
Harrison TM, Armstrong RL, Naeser CW, Harakal JE (1979) Geochronology and thermal history of the Coast Plutonic complex, near Prince Rupert BC Can J Earth Sci 16:400–410
Heitzmann P (1975) Zur Metamorphose und Tektonik im südöstlichen Teil der Lepontinischen Alpen. Schweiz Mineral Petrogr Mitt 55:467–522
Hunziker JC (1969) Rb/Sr Altersbestimmungen aus den Walliser Alpen Hellglimmer- und Gesamtgesteinsalterwerte. Eclogae Geol Helv 62:527–542
Hunziker JC (1970) Polymetamorphism in the Monte Rosa, Western Alps. Eclogae Geol Helv 63:151–161
Hunziker JC (1974) Rb/Sr and K/Ar age determination and the Alpine tectonic history of the Western Alps. Mem Ist Geol Mineral Univ Padova, 31
Hurford AJ, Green PF (1982) A users' guide to fission track dating calibration. Earth Planet Sci Letts 59:343–354
Hurford AJ, Green PF (1983) The zeta age calibration of fission track dating. Isot Geosci 1:285–317
Jäger E (1970) Rb/Sr systems in different degrees of metamorphism. Eclogae Geol Helv 63:163–172
Jäger E (1973) Die alpine Orogenese im Lichte der radiometrischen Altersbestimmung. Eclogae Geol Helv 66:11–21
Jäger E (1979) Introduction to geochronology. In: Jäger E, Hunziker JC (eds) Lectures in isotope geology. Springer, Berlin Heidelberg New York, pp 1–12
Jäger E, Niggli E, Wenk E (1967) Rb/Sr Altersbestimmungen an Glimmern der Zentralalpen. Beitr Geol Karte Schweiz NF 134, pp 67
Jäger E, Hunziker JC, Graeser S, Grünenfelder M (1969) Unpublished Field Guide for Coll. on Geochron. Phanerozoic Orogenic Belts, Switzerland
Jeanrichard F (1975) Summary of geodetic studies of recent crustal movements in Switzerland. Tectonophysics 29:289–292
Köppel V, Grünenfelder M (1975) Concordant U/Pb ages of monazite and xenotime from the Central Alps and the timing of high temperature Alpine metamorphism: a preliminary report. Schweiz Mineral Petrogr Mitt 55:129–132
Köppel V, Grünenfelder M (1978) The significance of monazite U/Pb ages: examples from the Lepontine area of the Swiss Alps. In: Zartman RE (ed) Short papers of the 4th Int Conf Geochron Cosmochron Isotope Geol US Geol Surv Open File Report 78–701, pp 226–227
Krishnaswami S, Lal D, Prabhu N, MacDougall D (1974) Characteristics of fission tracks in zircon: applications to geochronology and cosmology. Earth Planet Sci Letts 22:51–59
Lal D, Murali AV, Rajan RS, Tamhane AS, Lorin JC, Pellas P (1968) Techniques for proper revelation and viewing of etch tracks in meteoritic and terrestrial materials. Earth Planet Sci Letts 5:111–119
Milnes AG (1974) Structure of the Pennine zone (Central Alps): a new working hypothesis. Bull Geol Soc Am 85:1727–1732
Milnes AG (1978) Structural zones and continental collision, Central Alps. Tectonophysics 47:369–392
Milnes AG, Pfiffner OA (1977) Structural development of the Infrahelvetic complex, Eastern Switzerland. Eclogae Geol Helv 70:83–95
Naeser CW (1979) Fission track dating and geologic annealing of fission tracks. In: Jäger E, Hunziker JC (eds) Lectures in Isotope Geology. Springer, Berlin Heidelberg New York, pp 154–169
Naeser CW, Faul H (1969) Fission track annealing in apatite and sphene. J Geophys Res 74:705–710
Naeser CW, Izett GA, Obradovich JD (1980) Fission track and K/Ar ages of natural glasses. Bull US Geol Surv 1489, pp 31
Neugebauer HJ, Brotz R, Rybach L (1980) Recent crustal uplift and the present stress field of the Alps along the Swiss Geotraverse Basel-Chiasso. Eclogae. Geol Helv 73:489–500
Niggli E (1970) Alpine Metamorphose und alpine Gebirgsbildung. Fortschr Mineral 47:16–26
Purdy JW, Jäger E (1976) K/Ar ages on rock-forming minerals from the Central Alps. Mem Ist Geol Mineral Univ Padova, 30

Rybach L, Müller S, Milnes AG, Ansorge J, Bernoulli D, Frey M (1980) The Swiss geotraverse Basel-Chiasso – a review. Eclogae Geol Helv 73:437–462

Schaer JP, Reimer GM, Wagner GA (1975) Actual and ancient uplift rate in the Gotthard region, Swiss Alps: a comparison between precise levelling and fission track apatite age. Tectonophysics 29:293–300

Schmid SM, Zingg A, Handy M (1986) The kinematics of movements along the Insubric Line and the emplacement of the Ivrea zone (in press)

Schumacher E (1975) Herstellung von >99.9997% ^{38}Ar für die ^{40}K/^{40}Ar Geochronologie. Chimia 29:441–442

Siegenthaler R (1984) Alter und Geochemie von Glimmern und Feldspäten. Unpublished doctoral thesis, University of Berne

Steiger R (1964) Dating of orogenic phases in the Central Alps by K/Ar ages of hornblende. J Geophys Res 69:5407–5421

Steiger RH, Jäger E (1977) Subcommission on geochronology: convention on the use of decay constants in geo- and cosmochronology. Earth Planet Sci Lett 36:359–362

Steinitz G, Jäger E (1981) Rb/Sr and K/Ar studies on rocks from the Suretta nappe, Eastern Switzerland. Schweiz Mineral Petrogr Mitt 61:121–131

Trümpy R (1975) On crustal subduction in the Alps. In: Mahel M (ed) Tectonic problems of the Alpine system. Slovak Acad Sci, Bratislava, pp 121–130

Trümpy R (1980) Geology of Switzerland – a guide book. Part A: An outline of the geology of Switzerland. Wepf, Basel, pp 104

Turner DL, Forbes RB (1976) K/Ar studies in two deep basement drillholes: a new estimate of argon blocking temperature for biotite. Trans Am Geophys Union 57:353

Verschure RH, Andriessen PAM, Boelrijk NAIM, Hebeda EH, Maijer C, Priem HNA, Verdurmen EATh (1980) On the thermal stability of Rb/Sr and K/Ar biotite systems: evidence from coexisting Sveconorwegian (ca 870 Ma) and Caledonian (ca 400 Ma) biotites in SW Norway. Contrib Mineral Petrol 74:245–252

Vogler WS, Voll G (1981) Deformation and metamorphism at the south margin of the Alps, East of Bellinzona, Switzerland. Geol Rund 70:1232–1262

Wagner GA (1968) Fission track dating of apatites. Earth Planet Sci Lett 4:411–415

Wagner GA (1969) Spuren der spontanen Kernspaltung des ^{238}Urans als Mittel zur Datierung von Apatiten und ein Beitrag zur Geochronologie des Odenwaldes. N Jahrb Mineral Abh 110:252–286

Wagner GA, Reimer GM (1972) Fission track tectonics: the tectonic interpretation of fission track apatite ages. Earth Planet Sci Lett 14:263–268

Wagner GA, Reimer GM, Jäger E (1977) Cooling ages derived by apatite fission track, mica Rb/Sr and K/Ar dating: the uplift and cooling history of the Central Alps. Mem Ist Geol Mineral Univ Padova, 30

Wenk E, Keller F (1969) Isograde in Amphibolitserien der Zentralalpen. Schweiz Mineral Petrogr Mitt 49:157–198

Werner D (1980) Probleme der Geothermik im Bereich der Schweizer Zentralalpen. Eclogae Geol Helv 73:513–525

Zeitler P, Tahirkheli RAK, Naeser CW, Johnson NM (1982) Unroofing history of a suture zone in the Himalaya of Pakistan by means of fission track annealing ages. Earth Planet Sci Lett 57:227–240

Zingg A (1983) The Ivrea and Strona-Ceneri Zones (Southern Alps, Ticino and N. Italy) – a review. Schweiz Mineral Petrogr Mitt 63:361–392

Received July 17, 1985 / Accepted November 4, 1985